ARTICLE

Precise sample metering method by coordinated burst action of hydrophobic burst valves applied to dried blood spot collection

cReceived 00th January 20xx,
Accepted 00th January 20xx

DOI: 10.1039/x0xx00000x

Dries Vloemans[†a], Lorenz Van Hileghem[†a], Wannes Verbist [a], Debby Thomas [b], Francesco Dal Dosso[a] and Jeroen Lammertyn*[a]

Dried blood spot (DBS) sampling by finger-pricking has recently gained a lot of interest as alternative sample collection method. The reduced invasiveness, requirement of lower sample volumes and suitability for long-term storage at room temperature make DBS ideal for use in home settings or low-resource environments. However, traditional protocols often suffer from biased analysis data due to variable and not exactly known blood volumes present in the samples. In this work, a novel device has been developed to split-off precisely metered volumes from a blood drop and load them on pre-cut filter paper. Hereto, hydrophobic burst valves (HBV) were developed to temporarily retain a fluid flow, configurable to burst at pressures within a range of 175-600 Pa. By combining HBVs with different burst pressures, a volume metering system was developed to allow parallel metering of multiple pre-defined sample volumes. The system was shown to be accurate and consistent for blood volumes between 5-15 µL and for hematocrit levels spanning the range of 25-70%. Finally, a point-of-care DBS sampling device was developed combining the self-powered microfluidic SIMPLE technology. To evaluate the system's practical applicability, a validation study in the context of therapeutic drug monitoring of biologicals was performed using adalimumab-spiked blood samples. Microfluidic DBS samples showed good performance compared to the traditional DBS method with improved recovery rates (86% over 62%). This innovative metering system, allowing for parallelization and integration with complex liquid manipulations, will greatly impact the field of robust sampling, sample preparation, storage and analysis at the point-of-care.

1. INTRODUCTION

Dried blood spot (DBS) sampling of capillary blood is a promising minimally invasive alternative to conventional venipuncture [1]. DBS sampling, exploited for the first time for new-born screening in the 1960s [2,3], has now shown its applicability in a multitude of areas like therapeutic drug monitoring (TDM) [4,5], pharmacokinetics [6,7] and diagnosis of infectious diseases (e.g. HIV) [8]. These applications take advantage of improved logistical convenience, reduced cost, automatable processing and analysis, and increased analyte stability [9,10].

Despite the advantages, the high variability in blood sample hematocrit (Hct) levels (ranging between 23 and 67%) among different groups of patients [4,11–13] induces biases in quantitative bioanalyses. In fact, as blood with different Hct levels spreads differently through filter paper as a direct consequence of its different viscosity [14–16], DBS sub-punches with the same area contain different blood volumes linked to the respective Hct levels. Denniff and Spooner characterized a difference in blood volume of 35% across a Hct range of 0.2-0.8 [12]. Additionally, since red blood cells (RBCs) tend to accumulate at the edges of the DBS (14% higher RBC concentration at edges compared to centre) [17], referred to as the volcano effect, applying larger blood volumes or taking sub-punches in the central versus peripheral area of the DBS will lead to different assay data [18,19]. Furthermore, the susceptibility of the DBS method to contamination is a frequently reported problem due to, for instance, impurities and cell debris from the finger and imperfect sealing from the environment [20].

Different approaches to overcome the Hct-dependent spreading issue were reported. The first solutions, including pre-cut DBS papers [21] or perforated DBS papers in combination with micropipettes or microcapillaries, [22] lack control over precise volume application and user-friendliness, respectively. Volumetric absorptive micro samplers (VAMS®) [23] form an interesting solution in this direction, however, trials indicated that the tool is still relatively fallible for poor sample loading, significantly altering the absorbed blood volume [24,25]. Another approach, the volumetric absorptive paper disc (VAPD) and its downscaled version (VAPD-mini), sought to tackle the Hct effect by combining the VAMS principle with traditional DBS [26]. However, to circumvent user-dependency, direct finger contact during sample loading must be avoided. Therefore, improved strategies combine a microfluidic metering concept with the

[a] KU Leuven, Department of Biosystems - Biosensors Group, Willem de Croylaan 42, box 2428, 3001 Leuven, Belgium.
[b] KU Leuven, Department of Pharmaceutical and Pharmacological Sciences, Herestraat 49, box 424, 3000 Leuven, Belgium
†These authors contributed equally
* Corresponding author: jeroen.lammertyn@kuleuven.be; +3216321459

Electronic Supplementary Information (ESI) available: [file with detailed information on the used experimental setups, results of gravimetric characterization, burst pressure characterization and ELISA measurements and 4 videos illustrating the working principle of the single and parallel metering mechanism and the integrated SIMPLE-DBS sampling device]. See DOI: 10.1039/x0xx00000x

Please do not adjust margins

capillary action of a collection channel, allowing whole-spot analysis. The HemaXis DB device [27] and the Vacutainer qDBS card [28] are important examples here, showing volumetric loading of capillary blood in the range of 5-13.5 µL. Possible disadvantages in terms of contamination are conceivably improved by Neto et al. as they combined glass capillaries with pre-punched filter papers in a closed, pen-like handler, the HemaPEN [29]. Though, it only allows for sampling small volumes of 3 µL which limits its application in case multiple assays are needed, or for assays that require larger sample volumes. Altogether, current microfluidic techniques are based on the capillary interaction of the sample itself and do not allow parallel loading of different DBS from a single blood drop or further downstream processing of the sample.

In this work, a passive, low-cost and user-friendly microfluidic DBS sampling device (SIMPLE-DBS) is presented, utilizing coordinated burst actions of hydrophobic burst valves (HBVs) with configurable burst pressures. Hereto, the influence of two fluorinated solutions coated on specific channel regions on the contact angle and burst pressure is assessed. The HBVs enable parallel metering of predefined blood volumes starting from an unknown sample volume, ideal for multiplexed analyses on the same sample. To bring this concept at the point-of-care (POC) in a portable and autonomous device, the HBV-based metering system is integrated with our established SIMPLE platform with integrated pre-cut DBS papers [30–32]. To prove not only the technical advantages but also the improved clinical performance (e.g. recovery rate), our system is validated in the context of TDM of biologicals comparing it with the current traditional DBS method (e.g. Whatman 903 card) using citrated blood samples spiked with adalimumab (ADM).

2. MATERIALS AND METHODS

2.1. Reagent and materials

Whatman quantitative filter paper grades 43 and 598 (with respective thicknesses of 220 and 320 µm), Whatman 903 protein saver cards, sulphuric acid (H_2SO_4) and horseradish peroxidase (HRP) were obtained from Sigma-Aldrich (Belgium). Whatman qualitative filter paper grade CF12 was purchased from GE Healthcare (Belgium). Merck (Germany) delivered the peroxide (H_2O_2) and the o-phenylenediamine was obtained from Acros Organics (Belgium). PVC plastic films of 180 µm thickness were bought from Delbo (Belgium). Double-sided pressure-sensitive adhesive (PSA) tape (200MP 7956MP) and transfer tape (467MP) were acquired from 3M (USA). Aquapel and Fluoropel 800M hydrophobic agents were purchased from Aquapel (USA) and Cytonix (USA), respectively. Adalimumab (clone DE27) was acquired from Bio-rad laboratories (Belgium). Superblock™ T20 (PBS) blocking buffer was bought at Thermofisher Scientific (Germany). Monoclonal anti-ADM capture antibodies (MA-ADM28B8) and HRP-conjugated anti-ADM detection antibodies (MA-ADM40D8) were generated in-house at the Laboratory for Therapeutic and Diagnostic Antibodies (KU Leuven, Belgium) [33].

2.2. Microfluidic device fabrication

All microfluidic devices were fabricated using the low-cost and rapid lamination method proposed by Yuen. et al [34]. A microfluidic channel network was cut in a PSA layer using a digital craft cutter (Maxx Air 24 in., KNK, USA), and sealed with PVC films from the bottom and topside. The latter included the precut inlet, vent and prefilling holes. Single- and double-coated (sc/dc) HBVs were integrated by locally coating the bottom and/or top PVC film with hydrophobic fluorinated solutions (see Section 2.3). The Aquapel solution was also used to create the gas-permeable hydrophobic stop valves (HSV), as previously described [31]. In short, small rectangular patches (1.5 x 3 mm²) were cut in Whatman grade 43 or 598 filter paper, with a second craft cutter (Silhouette Cameo, Netherlands) and afterwards impregnated with Aquapel. The microfluidic devices used in Sections 3.3 and 3.4 were integrated with the self-powered SIMPLE pumping technology as driving source. In this technology, the wicking action of a working liquid in a paper substrate is exploited to generate pressure differences within the connected microfluidic network and, hence, to manipulate the liquid through it. For a more detailed explanation the reader is referred to our previous work [30,31,35,36]. The paper substrate (Whatman grade 598) of the SIMPLE pump module was cut with the Silhouette Cameo craft cutter and then inserted in its respective PSA chamber followed by sealing with the PVC films. The same craft cutter was used to cut the DBS paper (Whatman CF12) inserted in the integrated SIMPLE-based microfluidic DBS sampling device (SIMPLE-DBS, Section 3.4). After device assembly, the working liquid (1:20 diluted blue food dye in distilled water), acting as fuel of the pump module, was prefilled into the microfluidic device via the prefilling hole. The latter was finally sealed from the environment with a small PSA patch.

2.3. HBV fabrication

The surface properties of the microfluidic channels were locally altered by applying a hydrophobic fluorinated agent on the PVC surface via a mask-based coating strategy (Figure 1a). Hereto, a PSA mask with a rectangular cut-out (4 x 5 mm²) was applied to a PVC substrate (first rinsed with distilled water, then dried at room temperature) to retain the hydrophobic solution (Aquapel or Fluoropel). To ensure proper mask positioning, alignment markers were patterned on the PVC films during the cutting process. For the Aquapel treatment, 2 µL (0.1 µL/mm²) was applied, followed by a 1-hour incubation at 50 °C. For Fluoropel, 4 µL (0.2 µL/mm²) was used, followed by a 10 min incubation step at 50 °C and kept for at least 2 hours at room temperature before use. After drying, the PSA mask was removed from the PVC substrate. The Aquapel and Fluoropel coated substrates were integrated in a microfluidic channel as bottom to create a sc HBV or as bottom and top for the dc HBV (Figure 1b). Figure 1c shows the 5 different types of HBVs created by combining Aquapel and Fluoropel coatings

2.4. HBV characterization

Water contact angle measurements were performed to assess the hydrophobic properties and uniformity of the coated PVC

 This journal is © The Royal Society of Chemistry 20xx

Please do not adjust margins

Please do not adjust margins

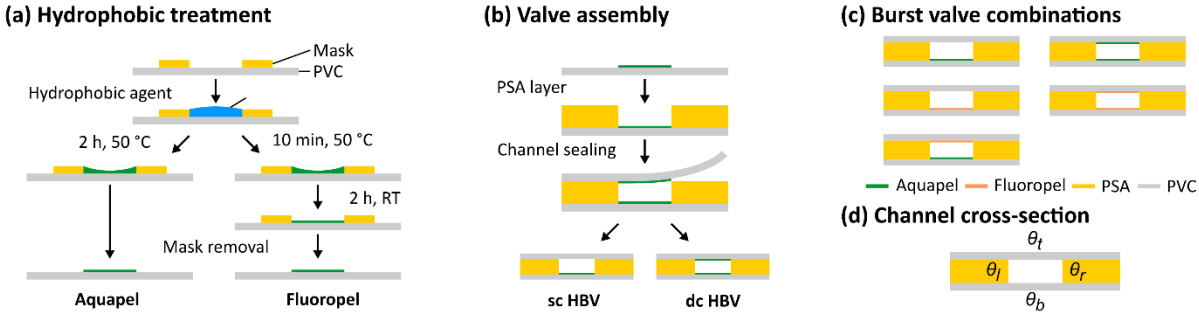

Figure 1: Schematic overviews of (a) mask-based hydrophobic treatment strategy of PVC with Aquapel and Fluoropel agent, (b) assembly of microfluidic channel to form sc and dc HBVs, (c) different types of HBVs using varying Aquapel-Fluoropel combinations at top and/or bottom of the channel, and (d) cross-section of microfluidic channel with different channel wall materials and contact angles.

substrates. To evaluate the homogeneity of the coating, a larger mask of 5 x 15 mm² was applied to the PVC substrate which was then coated with the respective Aquapel and Fluoropel hydrophobic agents. For each coating, 3 samples were prepared from which water contact angles were determined from at least 4 randomly positioned water droplets (5-10 µL) on the coated region using a CAM200 goniometer (KSV Instruments, Finland) and associated fitting software.

By combining the Fluoropel and Aquapel coatings, 5 different types of HBVs were formed as illustrated in Figure 1c. To evaluate the strength of each burst valve, the burst pressure of all coating combinations was experimentally determined and compared with theoretical values. The walls of the microfluidic channels have different water contact angles due to the layer-by-layer fabrication of different materials (Figure 1d). As a consequence, the extended Young-Laplace equation (Eq. (1)) was used to calculate the pressure difference within the channels: [37]

$$P_c = -\gamma\left(\left(\frac{\cos\theta_t + \cos\theta_b}{h}\right) + \left(\frac{\cos\theta_l + \cos\theta_r}{w}\right)\right) \qquad (1)$$

Here P_c [Pa] reflects the pressure difference (capillary pressure) over the liquid-air interface of the meniscus, γ [N/m] is the water surface tension and θ [°] with subscripts *t*, *b*, *l* and *r* is the contact angle of the top, bottom, left and right channel wall, respectively. *W* [m] and *h* [m] indicate the width and height of the channel.

Using Eq. (1), the burst pressure (ΔP_b [Pa]) of the HBVs was calculated as the difference of the capillary pressure from the untreated ($P_{c,1}$) and the hydrophobic treated channel part ($P_{c,2}$) with respective water contact angles of $\theta_{c,1}$ and $\theta_{c,2}$. As only the top and/or bottom of the channel were treated, the equation of the burst pressure (Eq. (2)) is given by:

$$\Delta P_b = -\gamma\left(\left(\frac{\cos\theta_{t,2} + \cos\theta_{b,2}}{h}\right) - \left(\frac{\cos\theta_{t,1} + \cos\theta_{b,1}}{h}\right)\right) \qquad (2)$$

where subscripts 1 and 2 indicate the untreated and treated channel part, respectively. By inserting the contact angles for θ_t and θ_b, in Eq.(2) the theoretical burst pressure for each type of HBV was calculated. From Eq. (2) follows that the burst pressure of the HBV is only influenced by the height and the hydrophobic properties of the bottom or/and top of the microchannel, while the channel width does not play a role (see Section SI.4 Supplementary Information for more details).

To experimentally determine the burst pressure of each HBV type, a pressure pump (LINEUP FLOW EZ™ SERIES 1000 mBar, Fluigent, France) was connected to a microfluidic channel having a width of 1.0 mm with incorporated HBV (fabricated as described in Section 2.2 and 2.3) and used to inject distilled water. The flow was maintained at a constant rate of 2 µL/min via an attached flow rate sensor (Flow unit M, Fluigent, France), while the applied pressure was recorded in real-time at 10 Hz. The burst pressure was obtained by taking the average pressure increase in the time interval in which the liquid meniscus is moving through the HBV after normalizing the absolute pressure to the baseline pressure. The latter refers to the required pressure to push the liquid through the channel without HBV (for more details, see Section SI.1 of the Supplementary Information). Tukey multiple comparison tests were performed to determine significant differences between the different mean burst pressures.

2.5. Sample metering system characterization

Citrated human whole blood was collected from healthy volunteers via venous puncture, after signing an informed consent form, and was processed within 24 hours of withdrawal. All experiments were approved by the UZ/KU Leuven Ethics Committee, Belgium (S62134). The blood was aliquoted in 2 mL samples and centrifuged at 2400 g for 15 minutes to separate the RBCs from the plasma. The plasma fraction in the samples was removed and volumetrically quantified from the aliquots to determine the initial Hct level. The remaining RBCs were reconstituted with a defined volume of the extracted blood plasma to prepare blood samples with specific Hct levels of 25, 40, 55 and 70%.

The volumetric performance of the microfluidic metering system was assessed by a gravimetric method (see Section SI.2, Supplementary Information for setup and accuracy of the methodology). Microfluidic devices incorporating the metering system were fabricated and 20 µL of the blood sample was prefilled in a collection channel. A syringe pump (PHD 2000, Harvard Apparatus, USA) was used to drive the sample through the microfluidic network (Figure SI.2c, Supplementary Information) in which a metered volume was split from the sample and subsequently loaded on top of a circular Whatman grade CF12 paper substrate. The weight difference of the paper

Please do not adjust margins

Please do not adjust margins

was quantified using a high precision weighing balance (CPA124S, Sartorius, Germany) before and immediately after sample loading, assuming negligible weight loss due to evaporation. The relative mass difference was converted to volume units using the respective density of the measured sample, which were calculated based on the relative density of the plasma (1.025 g/µL) and RBC (1.125 g/µL) fractions, resulting in 1.050, 1.065, 1.080, and 1.095 g/µL for Hct levels of 25, 40, 55 and 70%, respectively. The accuracy and reproducibility of the metering system were determined in two ways: i) for 3 volumes, 5, 10 and 15 µL, using 40% Hct blood samples, and ii) for 4 Hct levels of 25, 40, 55 and 70% using a fixed target volume of 10 µL.

2.6. Validation of SIMPLE-DBS sampling device

To assess both the technical and the analytical system performance, a comparative study between the developed microfluidic SIMPLE-DBS sampling device, with integrated self-powered SIMPLE pumping unit (see Section 2.2), and traditional Whatman protein saver cards was executed. In particular, 16 SIMPLE-DBS devices were run with human citrated blood (40% Hct) spiked with different ADM concentrations of 0, 1, 4 and 16 µg/mL to prepare 10 µL metered DBS samples. Standard DBS samples were prepared by spotting (using a micropipette) 40 and 10 µL of the same citrated blood samples on traditional Whatman protein saver cards. All DBS samples were left open to the air at room temperature for 24 hours to ensure complete drying. For extracting the 40 µL spotted DBS samples, a 6 mm diameter disc was punched out the centre of the spot and transferred to a 1.5 mL Falcon tube holding 240 µL Superblock™ T20 (PBS) buffer. The samples were incubated under continuous shaking for 1 hour at 21 °C and 300 rpm, followed by a 5 min centrifugation step at 14.000 RCF. Finally, 180 µL of the supernatant was transferred to an Eppendorf tube and stored at -20 °C. Both the Whatman protein saver cards spotted with 10 µL and the SIMPLE-DBS samples were extracted as a whole, i.e. without taking a sub-punch from the blood spot, using the same protocol.

To quantify the ADM concentrations in the DBS samples, an in-house developed sandwich ELISA was used [33]. Briefly, 96-well plates were coated with the capturing antibody MA-ADM28B8 for 72 h at 4 °C and blocked with 1% bovine serum albumin (BSA) in PBS, after which the diluted DBS extract samples were incubated overnight at 4 °C. Detection was performed using the HRP conjugated detecting antibody MA-ADM40D8 at room temperature. The plate was then washed and developed with o-phenylenediamine and H_2O_2 in citrate buffer for signal generation. The enzymatic reaction was stopped with H_2SO_4 (4 M), followed by measuring the absorbance at 492 nm with an ELx808 Absorbance Microplate Reader (BioTek Instruments Inc., USA). Optical density values were interpolated from the standard curve to calculate the ADM concentrations in the DBS samples. Next, the recovery was calculated by dividing the measured ADM concentration by the theoretical ADM concentration in the 3 configurations (SIMPLE-DBS system, traditional 40 µL spotted Whatman protein saver cards and the 10 µL spotted cards).

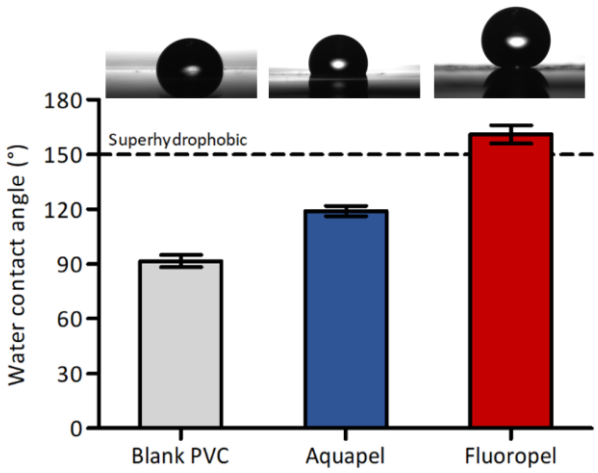

Figure 2: Bar chart indicating average water contact angles of the untreated and Aquapel, Fluoropel treated PVC substrates. For each condition 3 samples were prepared and the contact angles for at least 4 droplets were measured per sample. Error bars represent one standard deviation. The dotted line indicates the superhydrophobic region (>150°). Above each bar, a picture of such a measurement is shown for the respective coating.

3. RESULTS AND DISCUSSION

3.1. HBV characterization

The hydrophobic surface properties of the treated PVC substrates were analyzed for both Aquapel and Fluoropel agents and compared with the properties of the untreated PVC surface. As depicted in Figure 2, the water contact angle of untreated PVC (91.6 ± 3.4°) was increased to 119.0 ± 2.8° and 161.1 ± 5.0° for Aquapel and Fluoropel, respectively. The small standard deviations illustrate that both Fluoropel and Aquapel coatings led to homogenous properties over the entire treated region which were reproducible over multiple samples.

To characterize the burst pressures, five different types of HBVs were fabricated by combining the Aquapel and Fluoropel coatings as described in Section 2.3. In Figure 3a, the normalized average pressure profiles for sc Aquapel and dc Fluoropel-Aquapel HBVs are illustrated as an example. These profiles are in agreement with the expected pressure profile (Figure SI.1b, Supplementary Information), showing that the required pressure to maintain a constant flow rate, increases from the moment the meniscus of the liquid front reaches the HBV. Once the meniscus passes the full length of the HBV, the pressure drops again to its baseline pressure. As shown in Figure 3a, the required pressure to push a liquid over the dc Fluoropel-Aquapel HBV is significantly higher than the sc Aquapel HBV. The average burst pressure for each valve combination is summarized in Figure 3b (complete values are compiled in Table SI.1, Supplementary Information). The developed HBVs are configurable within a burst pressure range between ~175 and 600 Pa using a simple but robust approach without complex geometric features in the channel as mostly reported in literature [38]. Additionally, 4 out of the 5 valve types show a significant difference ($p<0.05$) in burst pressure which is

 This journal is © The Royal Society of Chemistry 20xx

Please do not adjust margins

Please do not adjust margins

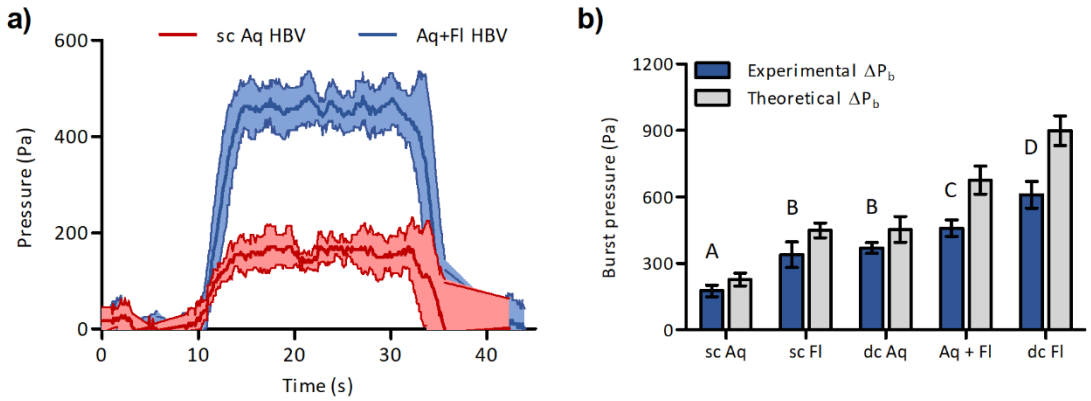

Figure 3: (a) Normalized average pressure profiles (solid lines) of sc Aquapel and dc Fluoropel-Aquapel HBVs. Shaded zones represent one standard deviation (n=6). (b) Theoretical vs. experimental burst pressures of the different HBVs in 1.0 mm wide microfluidic channels. Error bars represent one standard deviation (n ≥ 6). Different letters above bars indicate significant differences between the means (α = 0.05).

particularly interesting for enabling passive sequential liquid manipulations.

Figure 3b only illustrates the effect of the valve configuration (e.g. different combinations of hydrophobic coatings) on the burst pressure, while the relation between the microchannel dimensions (width and height) and burst pressure was evaluated in depth as well (Section SI.4, Supplementary Information). The obtained results are in agreement with Eq. (2) and confirm that only the channel height influences the burst pressure while the effect of the channel width was found to be negligible.

The experimentally determined burst pressures were also compared with their respective theoretical values (Figure 3b). These were calculated by inserting the obtained water contact angles (Section 3.1) of the untreated PVC and Aquapel/Fluoropel treated substrates in Eq. (2). As expected, a similar trend for the theoretical and experimental burst pressures for the five valve types was observed (Figure 3b), although, measured burst pressures are significantly lower. This discrepancy might be explained by the current manual coating and assembly process or the use of the static instead of dynamic contact angles in the theoretical calculations (see Supplementary Information Section SI.3) [39,40].

3.2. Sample metering system

Two of the four valve types (sc Aquapel and dc Aquapel-Fluoropel) presented in previous section were combined and integrated into a microfluidic system to enable the isolation and further manipulation of a precisely metered liquid volume from an unknown source volume. In Figure 4, the different steps of the metering workflow are shown. First, a droplet of red colored aqueous liquid is deposited on the inlet of the microfluidic

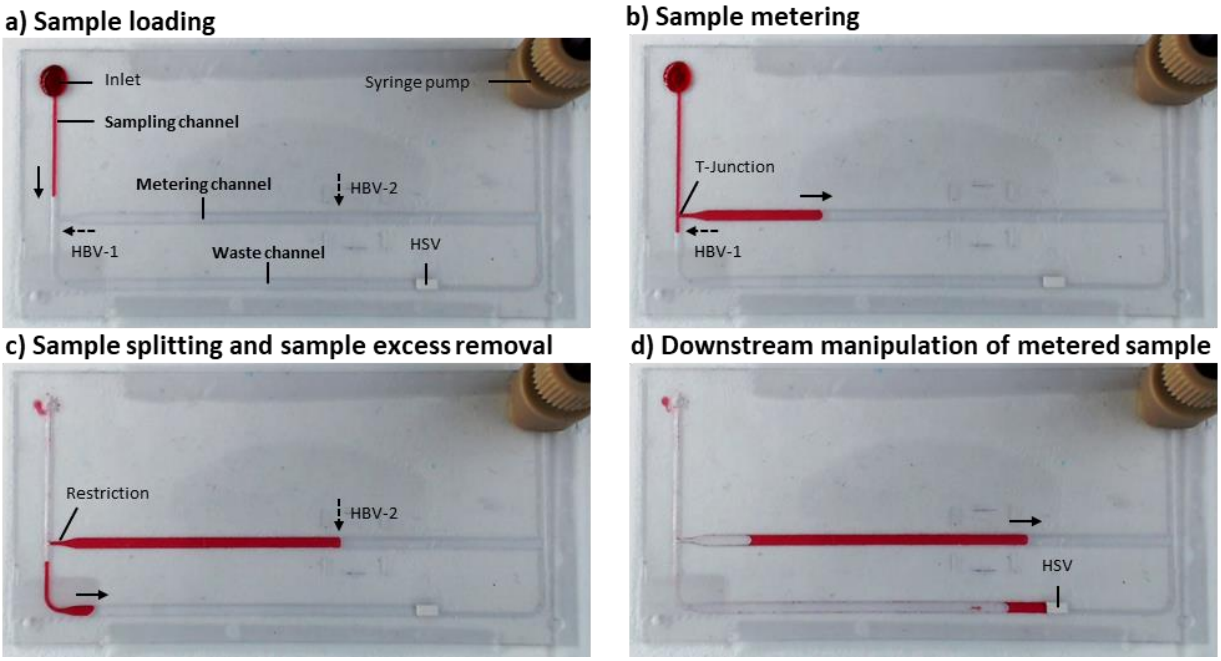

Figure 4: Working principle of sample metering system. (a) The sample is first loaded into the sampling channel until (b) its front meniscus reaches the T-junction where the sc HBV (HBV-1) directs the liquid into the metering channel. (c) Upon complete filling of the metering channel, the sample is blocked by dc HBV (HBV-2) leading to HBV-1 to burst and flowing of sample excess into the waste channel. As a result, the liquid in the metering channel becomes an isolated plug. (d) Finally, the HSV forces the metered sample liquid to burst through the HBV-2 and becomes available for downstream processes.

Please do not adjust margins

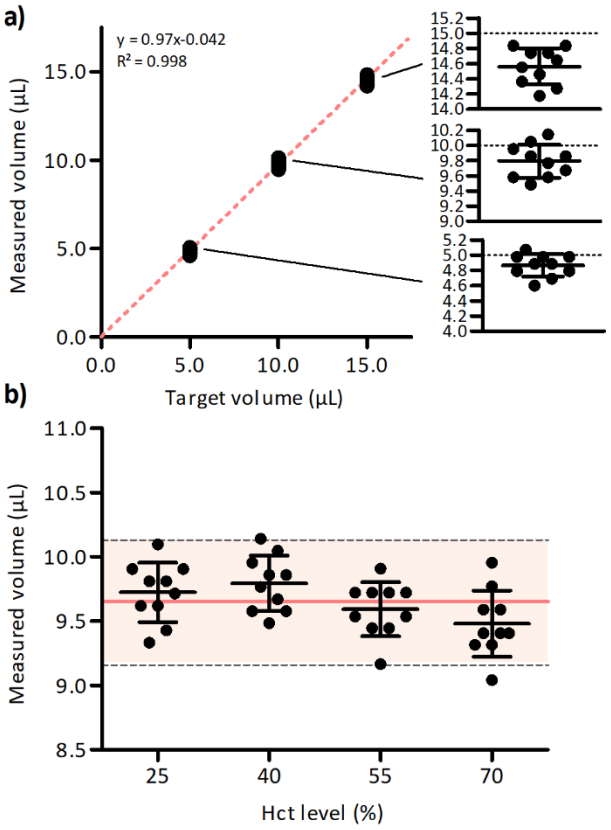

Figure 5: Gravimetric characterization of sample metering system. a) Measured vs. target volumes (5, 10 and 15 µL) of metered blood samples (Hct level of 40%) with close-ups of individual volume measurements (n=10) with mean and standard deviation for each target volume. b) Measurements of metered blood samples with different Hct levels of 25, 40, 55 and 70%. Solid red and dashed grey lines illustrate the global volume average (9.65 µL) over all Hct levels and 5% error zone around this average, respectively. For each Hct level, also separate averages (black lines) are given with error bars reflecting one standard deviation (n=10).

network. Next, the sample is drawn in the sampling channel by a syringe pump (Figure 4a, video SI.1 of Supplementary Information). A T-junction is located downstream the sampling channel, splitting the system into a metering and a waste channel. As the meniscus of the incoming sample liquid reaches this junction, a sc Aquapel HBV (HBV-1) directs the flow into the metering channel (Figure 4b). Upon complete filling of the metering channel, the sample is stopped by a dc Fluoropel-Aquapel HBV (HBV-2), which forces HBV-1 to burst according to the respective burst pressures. This way, the sample excess is directed into the waste channel until the receding liquid front reaches the T-junction and the excess volume splits from the metered plug (Figure 4c). Next, the sample excess is pulled to the end of the waste channel where a HSV blocks the flow. As a result, the isolated sample plug in the metering channel bursts through HBV-2 (Figure 4d) and the metered sample volume can then be further manipulated downstream.

Gravimetric measurements (video SI.2 of Supplementary Information) were performed to determine the volumetric performance of the metering system as exact blood volume metering and loading are key in DBS sampling to convert the measured analyte values to correct concentrations. The results of the gravimetric measurements (10 repetitions each), shown in Figure 5a, illustrate a good reproducibility (CV < 3%) of the metering system for each target volume (5, 10 and 15 µL). The high accuracy of the system was confirmed as well as the bias of the average metered volumes were found to deviate maximally 3% below the target volumes. This drop was expected to some extent because a small fraction of the sample liquid remains trapped in the channel walls imperfections. The bias between the measured and target volume slightly increases with larger target volumes (close ups in Figure 5a) confirming that the loss is proportional to the length of the channels, and, hence, this loss can be compensated for when designing the channel network. The overall good performance over the range of target volumes is confirmed by the good linear fit (R^2 = 0.99) to all gravimetric data points with a slope close to 1 as is illustrated in Figure 5a (see Table SI.4 in Supplementary Information for the values). To even further improve the accuracy and reproducibility, the system would benefit from automated fabrication methods such as roll-to-roll manufacturing and micropatterning techniques. Consequently, channels with higher resolution and better alignment of the hydrophobic patches and different plastic layers can be achieved.

Similar gravimetric measurements were performed to evaluate the Hct-dependency of the microfluidic metering system. As the Hct levels between different patients can show large variability, the analyzed results from traditional DBS sampling methods often show bias and cannot be trusted [17,41]. To account for these variations, the Hct levels were varied between 25 and 70%, covering more than the typical physiological range for humans. The results (again 10 repetitions each) are depicted in Figure5b (and Table SI.4, Supplementary Information) showing no significant difference in measured volumes (target volume 10 µL) for 25, 40, 55 and 70% Hct levels. Remarkably, CV values below 3% were observed for all measurements indicating that a varying level of RBCs does not influence the reproducibility of the metering system. When all individual gravimetric measurements are compared to the global average (9.65 µL, represented by the full red line in Figure 5b), 95% (38 out of 40) of the data points are located within the 5% error zone around the mean (dashed grey lines in Figure 5b).

The data show a significant improvement to traditional methods, where a volume variability up to 29% was observed across a similar Hct range [12]. VAMS were shown to have a variability of 3.6% (CV%) [23], however, an inter-laboratory experiment showed a variability up to 8.7% (CV%) [24], illustrating the need for user-independent metering systems. Channel-based systems like the ones from Neto et al. and Lenk et al. show overall CVs of ≤ 3.0%, a threshold that is matched by our metering system [28,29].

3.3. Parallel sample metering on SIMPLE

To show the potential of the metering system in splitting a single sample drop in multiple liquid plugs of exact volume sizes, a microfluidic chip (Figure 6a) with 3 metering channels of different volumes (5, 10 and 15 µL) was designed. Here, the syringe pump was replaced by a SIMPLE unit acting as a passive driving source to manipulate the liquid through the system, showing the applicability of this concept at the POC. The working principle of the SIMPLE has been presented

This journal is © The Royal Society of Chemistry 20xx

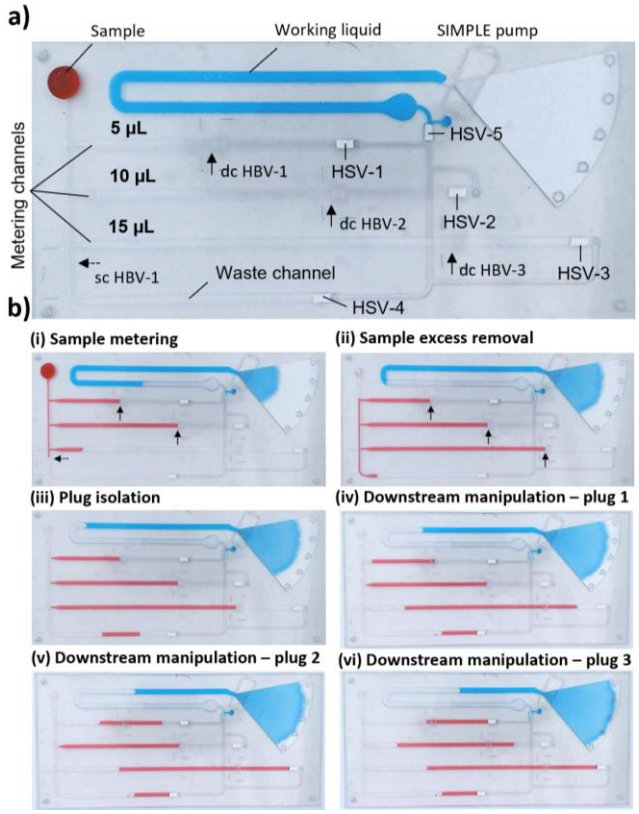

Figure 6: a) Microfluidic chip design for parallel sample metering with integrated SIMPLE unit. b) Snapshots of different liquid manipulation steps through the microfluidic system: (i) filling the metering channels by the sample, (ii) removal of the sample excess to the waste channel, (iii) isolation of the metered volume plugs and (iv-vi) subsequent bursting of each volume plug through the dc HBVs.

previously[31,32,35,36], but briefly, a triangular-shaped nitrocellulose porous substrate (Whatman grade 598) creates a negative pressure upon wicking in the prefilled working liquid (blue water in Figure 6). Hence, the sample is drawn into the inlet and through the metering system. Similar to the metering concept discussed in Section 3.2 above, a sc HBV first forces the incoming sample liquid to fill the metering channels, after which the sample excess is discarded to the waste channel. After removal of the sample excess, each individually isolated sample volume bursts through the dc HBV and is manipulated downstream until they reach the HSVs (see Figure 6b, and video SI.3 of Supplementary Information). An additional HSV (HSV-5) was inserted at the receding backside of the prefilled working liquid to direct the working liquid towards the porous paper upon finger-press activation.

The ability to split and further manipulate multiple precisely metered volumes in an autonomous way using SIMPLE technology opens the door to on-chip parallelization and much more advanced liquid manipulation compared to current solutions. The use of the SIMPLE unit as passive driving source, which operates as an external pressure source on the incoming sample, is the core benefit of the currently presented strategy. This makes the propulsion of the liquid independent of the sample-channel interaction as is the case for traditional capillary microfluidics [37,42].

3.4. Integrated volumetric SIMPLE-DBS sampling device

To translate the sample metering principle towards an integrated Hct-independent DBS sampling device that can be used at the POC, again a SIMPLE unit was integrated for liquid propulsion. This way, the SIMPLE-DBS sampling device (Figure 7) becomes completely autonomous and ideal for self-sampling in decentralized POC settings (e.g. patient's home). As consistent 'parallel loading' of multiple isolated volume plugs (possibility of parallel plug isolation itself was shown Section 3.3) on separate DBS papers requires novel technical

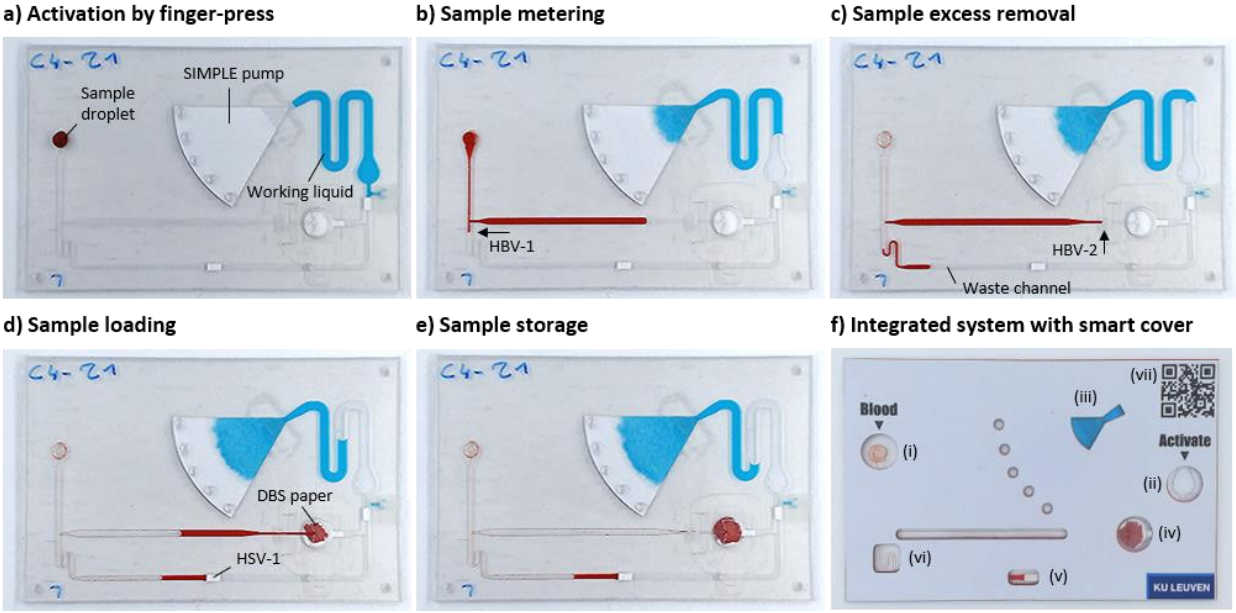

Figure 7: Snapshots of the working principle of the integrated microfluidic DBS sampling device. a) A drop of citrated-blood is applied at the inlet of the sampling channel and the system is activated by a single finger-press. b) The activated SIMPLE unit draws the blood sample in the microfluidic network. c) Upon complete filling of the metering channels, the sample excess is directed to the waste channel followed by (d) loading of both metered sample plugs on the DBS papers. e) Once loaded, the samples are stored on the chip for drying and transported to the laboratory for analysis. f) Cartridge of integrated DBS system with cover sticker, illustrating the different control zones for assessing successful chip performance.

Please do not adjust margins

innovations, which fall out of the scope of this work, the working principle of an integrated device with single DBS paper is shown. Furthermore, it is not expected that the analytical performance of the system will be influenced by moving towards multiple DBS samples. Hereto, a circular DBS paper (7 mm diameter, Whatman grade CF12) was incorporated in a second microfluidic layer underneath the metering system (Figure SI.5, Supplementary Information). Immediately downstream the DBS paper, an HSV (HSV-2) was placed to avoid the blood sample to be pulled out from the DBS paper. Also here, the working liquid is flanked by a HSV (HSV-3) to avoid the occurrence of backflow of the working liquid upon activation. After sample loading and drying, the DBS paper can be removed via a removable back-film (see section SI.6 of Supplementary Information), ready to be analyzed in clinical laboratories without the need of taking a sub-punch. The different phases of the integrated SIMPLE-DBS microfluidic device working principle are illustrated in Figure 7a-e (see also video SI.4 of the Supplementary Information). It is important to mention that all phases described are performed within 5 minutes and that this turnover time can be further reduced by increasing the pump flow rate (function of the angle and porosity of the paper) [35].

Figure 7f shows the final integrated SIMPLE-DBS system with an attached cover sticker making the device more intuitive and user-friendly for people without special training. The cover features indicate (i) where to apply the finger-prick blood drop, (ii) an activation spot for the SIMPLE pump, (iii) indicator of successful SIMPLE activation, (iv) windows to confirm successful loading of the metered sample volumes on the DBS papers, (v) a control zone to assess if sufficient sample volume was applied at the inlet to fill the metering channel (true if blood is visible), (vi) a second control zone to check successful splitting of the sample excess from the metered sample (true if no blood is visible), and (vii) a QR-code used for tracking each sampling device and possibly access to the patient's information. This QR-code can also be replaced by a zone available for written text.

3.5. Device validation with adalimumab-spiked blood samples

TDM of biologicals is an expanding field which would benefit from a reliable remote self-sampling DBS device. In fact, for ADM, world's bestselling drug and biological used to treat patients suffering from chronic autoimmune diseases (e.g. inflammatory bowel disease, rheumatoid arthritis), dosing is in practice not straightforward because of intra- and interpatient pharmacokinetic variability, leading to i) underexposure in case of sub-therapeutic serum drug concentrations or due to the production of neutralizing anti-drug antibodies [43–46], and ii) possible drug overexposure resulting in unnecessarily high therapy costs [47]. The DBS sampling method facilitates patients to routinely collect blood samples at home and send them via regular mail to a clinical laboratory for analysis, reaching a personalized treatment plan in a much more effective way.

In this context, the SIMPLE-DBS sampling device was compared to traditional Whatman protein saver cards to evaluate the system's performance for monitoring ADM concentrations in blood samples. To do so, ADM-spiked citrated blood samples corresponding to a clinically relevant concentration range (0, 1, 4 and 16 µg/mL) were used to prepare DBS samples with the SIMPLE-DBS device. For comparison, Whatman protein saver cards were loaded with a volume of 40 µL in combination with sub-punches as the standard method, while different cards were loaded with precisely 10 µL of blood as the whole-spot analysis reference.

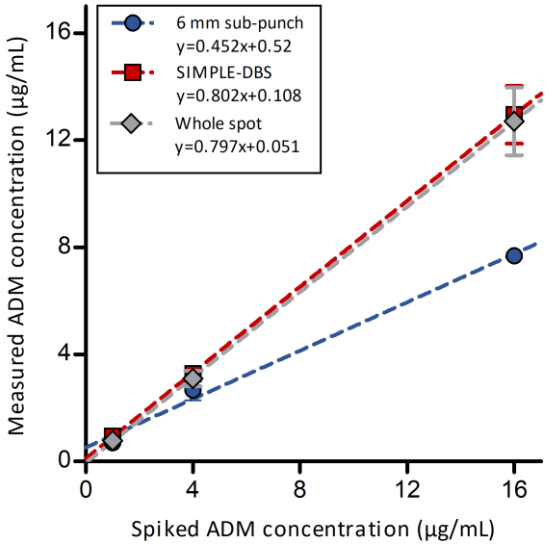

Figure 8: Calibration curves of the measured ADM concentrations for the different DBS sample preparation methodologies (6 mm sub-punch (n=9), SIMPLE-DBS (n=12) or whole spot (n=9)). Error bars represent one standard deviation around the mean ADM concentration. Linear fitted curves (R^2>0.96) are plotted as dashed lines through the data points of each DBS method.

All the extracted samples were analyzed with the ELISA reference technology as described in Section 2.6 from which the results are summarized in Figure 8 (exact values are given in Table SI.5). The graph shows that the fitted regression curves of the SIMPLE-DBS device and whole spot overlap (slope ~0.80), while the one of the 6 mm sub-punch methodology has a much lower slope of 0.452. This difference in slopes was determined to be strongly significant ($p < 0.0001$, F-test on the interaction effect between sampling method and spiked concentration, via general linear regression model (GLM)) and confirms the better performance of the developed SIMPLE-DBS device. Also when the average recovery rates of each methodology are evaluated, higher values are obtained for the SIMPLE-DBS and whole-spot analysis methodology (86% and 78%, respectively) compared to the 6 mm sub-punch one (62%). However, these are the average recovery rates taken over all concentrations and should be interpreted carefully as the GLM showed the recovery rates to be concentration dependent. Still, for each concentration a higher and more consist recovery rate is observed for the SIMPLE-DBS method (Table SI.5).

Conclusions

In this paper, a user-independent system for producing precisely metered dried blood spots was developed, characterized and integrated with a self-powered microfluidic pump (SIMPLE). First, hydrophobic burst valves were developed

This journal is © The Royal Society of Chemistry 20xx

Please do not adjust margins

Please do not adjust margins

to temporarily retain a liquid flow by locally coating the channels with Aquapel and Fluoropel. Applying these fluorinated compounds to obtain single and/or double coated channel sections, 4 significantly different burst pressures between 175 and 600 Pa were accomplished. The sequential burst actions of 2 hydrophobic burst valves with different burst pressures was then used to create a passive metering system. The accuracy and reproducibility of the system was evaluated for different metered blood volumes (5, 10 and 15 µL), as well as for a broad blood Hct range (25-70%). For both, gravimetric characterization showed CV values below 3%. The system's capability and flexibility to meter multiple different volumes starting from an unknown sample volume in an autonomous way was also shown by integration with the SIMPLE technology.

Next, the metering system was further implemented towards an autonomous and portable DBS sampling system, i.e. SIMPLE-DBS. In this approach, the blood sample was passively manipulated by SIMPLE through the metering system and subsequently loaded on a pre-cut DBS paper, embedded and sealed in the device to avoid any risk of contamination. Importantly, the system is adjustable to split-off multiple metered volumes in parallel within a range of 1-10's of microliters each from a single blood drop in parallel.

The performance of the integrated SIMPLE-DBS system was finally validated in the context of TDM for biologicals. Here, citrated blood samples spiked with clinically relevant adalimumab concentrations (0-16 µg/mL) were used to compare the SIMPLE-DBS system with the traditional Whatman protein saver card approach. The SIMPLE-DBS system showed an overall higher ADM recovery and equal reproducibility compared to the traditional 6 mm sub-punched DBS samples on Whatman protein saver cards. The results were in good agreement with the whole-spot 10 µL reference DBS samples.

The obtained results show the value of metered SIMPLE-DBS in combination with whole-spot analysis. Furthermore, the potential of the presented device to integrate this sample metering strategy in the current workflow for TDM was clearly demonstrated. Moreover, our system challenges the current state of the art by manipulating the sample with an external, passive driving source instead of relying solely on the capillary action of the sample in the microfluidic system. As a consequence, multiple metered volumes can be isolated in parallel from a single sample drop. This paper presents the first steps towards a novel method for preparing accurate DBS samples. Future work will focus on enabling parallel DBS loading and evaluating the influence of the Hct effect on the recovery efficiency. Furthermore, to make the device applicable for clinical field testing, a user-friendly chip-to-world interface has to be integrated which allows proper application of finger-prick capillary blood. Even more, we believe that our system is not restricted to sample collection but also allows for downstream manipulation of the metered sample, making it employable in a myriad of on-chip diagnostic POC applications.

Author Contributions

Dries Vloemans: Conceptualization, Experimental design and planning, Characterization, Validation, Formal analysis, Investigation, Writing – Original Draft, Visualization. Lorenz Van Hileghem: Conceptualization, Experimental design and planning, Characterization, Validation, Formal analysis, Investigation, Writing – Original Draft. Wannes Verbist, Characterization, Investigation. Debby Thomas: Resources, Writing – Review & Editing. Francesco Dal Dosso: Conceptualisation, Experimental design and planning, Writing – Review & Editing, Supervision, Funding acquisition, Project administration. Jeroen Lammertyn: Conceptualization, Resources, Writing - Review & Editing, Supervision, Funding acquisition, Project administration.

Conflicts of interest

There are no conflicts to declare.

Acknowledgements

This work was supported by the Research Foundations – Flanders (FWO G086114N, SB project 1S33618N) and the KU Leuven (C3 project C32/17/007, C2 project C24/16/022, ID-N project IDN/20/011, IOF mandate 3E160311). Furthermore, we thank Sophie Tops and Griet Compernolle (Laboratory for Therapeutic and Diagnostic Antibodies, KU Leuven, Belgium) for performing the DBS extractions and ELISAs.

Notes and references

1 B. U. W. Lei and T. W. Prow, *Biomed. Microdevices*, 2019, **21**, 1–30.
2 I. Bang, *Biochem. Ztschr.*, 1913, **49**, 19–39.
3 R. Guthrie and A. Susi, *Pediatrics*, 1963, **32**, 338–43.
4 A. J. Wilhelm, J. C. G. den Burger, R. M. Vos, A. Chahbouni and A. Sinjewel, *J. Chromatogr. B Anal. Technol. Biomed. Life Sci.*, 2009, **877**, 1595–1598.
5 S. Velghe, L. Delahaye and C. P. Stove, *J. Pharm. Biomed. Anal.*, 2019, **163**, 188–196.
6 M. Rowland and G. T. Emmons, *AAPS J.*, 2010, **12**, 290–293.
7 C. M. Nijenhuis, A. D. R. Huitema, S. Marchetti, C. Blank, J. B. A. G. Haanen, J. V. van Thienen, H. Rosing, J. H. M. Schellens and J. H. Beijnen, *J. Clin. Pharmacol.*, 2016, **56**, 1307–1312.
8 K. Sikombe Id, K. Musukuma Id, A. Sharma, N. Padian, C. Holmes, N. Czaicki, S. Simbeza, P. Somwe, C. Bolton-Moore, I. Sikazwe and E. Geng, *PLoS One*, 2019, 1–14.
9 P. Van Amsterdam and C. Waldrop, *Bioanalysis*, 2010, **2**, 1783–1786.
10 L. C. Martial, R. E. Aarnoutse, M. F. Schreuder, S. S. Henriet, R. J. M. Brüggemann and M. A. Joor, *PLoS One*, 2016, 1–17.
11 P. Timmerman, S. White, S. Globig, S. Lüdtke, L. Brunet and J. Smeraglia, *Bioanalysis*, 2011, **3**, 1567–1575.
12 P. Denniff and N. Spooner, *Bioanalysis*, 2010, **2**, 1385–1395.

This journal is © The Royal Society of Chemistry 20xx

Please do not adjust margins

Please do not adjust margins

13 P. M. M. De Kesel, N. Sadones, S. Capiau, W. E. Lambert and C. P. Stove, *Bioanalysis*, 2013, **5**, 2023–2041.
14 P. Abu-Rabie, P. Denniff, N. Spooner, B. Z. Chowdhry and F. S. Pullen, *Anal. Chem*, 2015, **87**, 4996–5003.
15 G. F. Carter, *Br. J. Ind. Med.*, 1978, **35**, 235–240.
16 T. C. Chao, O. Arjmandi-Tash, D. B. Das and V. M. Starov, *J. Colloid Interface Sci.*, 2015, **446**, 218–225.
17 D. F. Stickle, N. J. Rawlinson and J. D. Landmark, *Clin. Chim. Acta*, 2009, **401**, 42–45.
18 S. J. Moat, C. Dibden, L. Tetlow, C. Griffith, J. Chilcott, R. George, L. Hamilton, T. H. Wu, F. MacKenzie and S. K. Hall, *Bioanalysis*, 2020, **12**, 99–109.
19 M. O'Mara, B. Hudson-Curtis, K. Olson, Y. YueH, J. Dunn and N. Spooner, *Bioanalysis*, 2011, **3**, 2335–23347.
20 M. Resano, M. A. Belarra, E. García-Ruiz, M. Aramendía and L. Rello, *TrAC - Trends Anal. Chem.*, 2018, **99**, 75–87.
21 N. Youhnovski, A. Bergeron, M. Furtado and F. Garofolo, *Rapid Commun. Mass Spectrom.*, 2011, **25**, 2951–2958.
22 F. Li, S. Ploch, D. Fast and S. Michael, *J. Mass Spectrom.*, 2012, **47**, 655–667.
23 N. Spooner, P. Denniff, L. Michielsen, R. De Vries, Q. C. Ji, M. E. Arnold, K. Woods, E. J. Woolf, Y. Xu, V. Boutet, P. Zane, S. Kushon and J. B. Rudge, *Bioanalysis*, 2015, **7**, 653–659.
24 P. Denniff and N. Spooner, *Anal. Chem*, 2014, **86**, 8489–8495.
25 G. Fuller, K. Njune Mouapi, S. Joung, C. Shufelt, I. van den Broek, M. Lopez, S. dhawan, M. Mastali, C. Spiegel, N. Bairey Merz, J. E. Van Eyk and A. Robinson, *Biodemography Soc. Biol.*, 2019, **65**, 313–322.
26 T. Nakahara, N. Otani, T. Ueno and K. Hashimoto, *J. Chromatogr. B Anal. Technol. Biomed. Life Sci.*, 2018, **1087**–**1088**, 70–79.
27 L. A. Leuthold, O. Heudi, J. Déglon, M. Raccuglia, M. Augsburger, F. Picard, O. Kretz and A. Thomas, *Anal. Chem.*, 2015, **87**, 2068–2071.
28 G. Lenk, S. Sandkvist, A. Pohanka, G. Stemme, O. Beck and N. Roxhed, *Bioanalysis*, 2015, **7**, 2085–2094.
29 R. Neto, A. Gooley, M. C. Breadmore, E. F. Hilder and F. Lapierre, *Anal. Bioanal. Chem.*, 2018, **410**, 3315–3323.
30 T. Kokalj, Y. Park, M. Vencelj, M. Jenko and L. P. Lee, *Lab Chip*, 2014, **14**, 4329–33.
31 F. Dal Dosso, L. Tripodi, D. Spasic, T. Kokalj and J. Lammertyn, *ACS Sensors*, 2019, **4**, 694–703.
32 F. Dal Dosso, D. Decrop, E. Pérez-Ruiz, D. Daems, H. Agten, O. Al-Ghezi, O. Bollen, J. Breukers, F. De Rop, M. Katsafadou, J. Lepoudre, L. Lyu, P. Piron, R. Saesen, S. Sels, R. Soenen, E. Staljanssens, J. Taraporewalla, T. Kokalj, D. Spasic and J. Lammertyn, *Anal. Chim. Acta*, 2018, **1000**, 191–198.
33 S. Bian, T. Van Stappen, F. Baert, G. Compernolle, E. Brouwers, S. Tops, A. de Vries, T. Rispens, J. Lammertyn, S. Vermeire and A. Gils, *J. Pharm. Biomed. Anal.*, 2016, **125**, 62–67.
34 P. K. Yuen and V. N. Goral, *Lab Chip*, 2010, **10**, 384–387.
35 F. Dal Dosso, Y. Bondarenko, T. Kokalj and J. Lammertyn, *Sensors Actuators, A Phys.*, 2019, **287**, 131–137.
36 F. Dal Dosso, T. Kokalj, J. Belotserkovsky, D. Spasic and J. Lammertyn, *Biomed. Microdevices*, 2018, **20**, 1–11.
37 A. Olanrewaju, M. Beaugrand, M. Yafia and D. Juncker, *Lab Chip*, 2018, **18**, 2323–2347.
38 B. Hagmeyer, F. Zechnall and M. Stelzle, *Biomicrofluidics*, 2014, **8**, 1–9.
39 M. Bauer, M. Ataei, M. Caicedo, K. Jackson, M. Madou and L. Bousse, *Microfluid. Nanofluidics*, 2019, **23**, 1–12.
40 J. H. Kim, P. Kavehpour and J. P. Rothstein, *Phys. Fluids*, 2015, **27**, 1–7.
41 G. Lenk, S. Ullah, G. Stemme, O. Beck and N. Roxhed, *Anal. Chem.*, 2019, **91**, 5558–5565.
42 L. Gervais and E. Delamarche, *Lab Chip*, 2009, **9**, 3330–3337.
43 C. Bastida, V. Ruíz, M. Pascal, J. Yagüe, R. Sanmartí and D. Soy, *Br. J. Clin. Pharmacol.*, 2017, **83**, 962–975.
44 F. Baert, M. Noman, S. Vermeire, G. Van Assche, G. D'Haens, A. Carbonez and P. Rutgeerts, *N. Engl. J. Med.*, 2003, **348**, 601–608.
45 A. A. Fasanmade, O. J. Adedokun, J. Ford, D. Hernandez, J. Johanns, C. Hu, H. M. Davis and H. Zhou, *Eur. J. Clin. Pharmacol.*, 2009, **65**, 1211–28.
46 A. A. Fasanmade, O. J. Adedokun, M. Blank, H. Zhou and H. M. Davis, *Clin. Ther.*, 2011, **33**, 946–964.
47 S. D. Undevia, G. Gomez-Abuin and M. J. Ratain, *Nat. Rev. Cancer*, 2005, **5**, 447–458.

This journal is © The Royal Society of Chemistry 20xx

Please do not adjust margins